Snapshot Mueller matrix polarimeter by wavelength polarization coding

Matthieu Dubreuil, Sylvain Rivet, Bernard Le Jeune

Snapshot Mueller matrix polarimeter by wavelength polarization coding

Matthieu Dubreuil, Sylvain Rivet*, Bernard Le Jeune, and Jack Cariou

Laboratoire de Spectrométrie et Optique Laser (E.A. 938), Université de Bretagne Occidentale, 6 Avenue le Gorgeu, C.S. 93837, 29238 Brest Cedex, France
**Corresponding author: sylvain.rivet@univ-brest.fr*

http://www.opticsexpress.org

Abstract: We present a new, to the best of our knowledge, experimental configuration of Mueller matrix polarimeter based on wavelength polarization coding. This is a compact and fast technique to study polarization phenomena. Our theoretical approach, the necessity to correct systematic errors and our experimental results are presented. The feasibility of the technique is tested on vacuum and on a linear polarizer.

OCIS codes: (230.5440) Polarization-sensitive device; (260.5430) Polarization

References and links

1. B. Boulbry, B. Bousquet, B. Le Jeune, Y. Guern, and J. Lotrian, "Polarization errors associated with zero-order achromatic quarter-wave plates in the whole visible spectral range," Opt. Express **9**, 225-235 (2001).
2. B. Boulbry, T. A. Germer, and J. C. Ramella-Roman, "A novel hemispherical spectro-polarimetric scattering instrument for skin lesion imaging," Proc. SPIE **6078**, 128-134 (2006).
3. C. Baravian, J. Dillet, F. Caton, and J.P. Decruppe, "Birefringence determination in turbid media," Phys. Rev. E **75**, 032501 (2007).
4. F Boulvert, B Boulbry, G Le Brun, B Le Jeune, S Rivet, and J Cariou , "Analysis of the depolarizing properties of irradiated pig skin," J. opt. A, Pure appl. opt. **7**, 21-28 (2005).
5. S. Guyot, M. Anastasiadou, E. Deléchelle, and A. De Martino, "Registration scheme suitable to Mueller matrix imaging for biomedical applications," Opt. Express **15**, 7393-7400 (2007).
6. J. W. Evans,, "Solc biregringent filter," J. Opt. Soc. Am. **48**, 142-146 (1958).
7. K. Oka and T. Kato, "Spectroscopic polarimetry with a channeled spectrum," Opt. Lett. **24**, 1475-1477 (1999).
8. N. A. Hagen, D. S. Sabatke, J. F. Scholl, P. A. Jansson, W. W. Chen, E. L. Dereniak, and D. T. Sass, "Compact methods for measuring stress birefringence," Proc. SPIE **5158**, 45-53 (2003).
9. N. Hagen, K. Oka, and E. L. Dereniak, "Snapshot Mueller matrix spectropolarimeter," Opt. Lett. **32**, 2100-2102 (2007).
10. G. Ghosh, "Dispersion-equation coefficients for the refractive index and birefringence of calcite and quartz crystals," Opt. Comm. **163**, 95-102 (1999).

1. Introduction

Mueller matrix polarimetry allows one to determine the full polarimetric response of a medium, using light as a non-invasive investigation technique. Nevertheless the current polarimeters are not able to measure Mueller matrices instantaneously [1,2], which limits the application field of polarimetry. Indeed a snapshot polarimeter could study quick phenomena like complex fluids [3] for instance or, on the contrary, avoid motions due to the patient during medical diagnosis [4,5].

Generally a Mueller polarimeter is composed of two polarimetric parts: one that successively generates several states of polarization before the medium, by rotating quarter wave plates or variable wave plates for instance, and another that analyses the state of polarization modified by the medium. The snapshot Mueller polarimeter works along the same scheme but its originality comes from the fact that the states of polarization are

generated simultaneously by each wavelength of a broadband spectral source. Polarization coding by wavelength is commonly found in birefringent filters [6] or in snapshot Stokes-Meters [7,8]. All these techniques use birefringent plates whose thickness and orientation enable to select a wavelength or to measure the Stokes vector. This paper presents the theoretical approach and experimental methodology to get a Mueller matrix based on this principle.

The paper will be organized as follows: firstly the principle of the snapshot Mueller polarimeter will be explained. Then we will describe the chosen experimental set-up. Finally, after specifying the corrections that must be made in the treatment of the spectrum, we will comment our experimental results for two standard media.

2. Theoretical approach

A lot of experimental configurations permit to extract instantaneously the elements of the Mueller matrix. The most basic one is composed of four birefringent plates of the same material and two linear polarizers. Its coding system is made of a linear polarizer at 0° and two wave plates with their optical axis respectively at 45° and 0°. The decoding system is made of two wave plates with their optical axis respectively at 0° and 45°, and a linear polarizer at 90°. The source has a broadband spectrum and the intensity spectrum is given by a spectrometer coupled with a CCD camera (Fig. 1). Since the information is measured by only one spectrum, acquisition time can be very short.

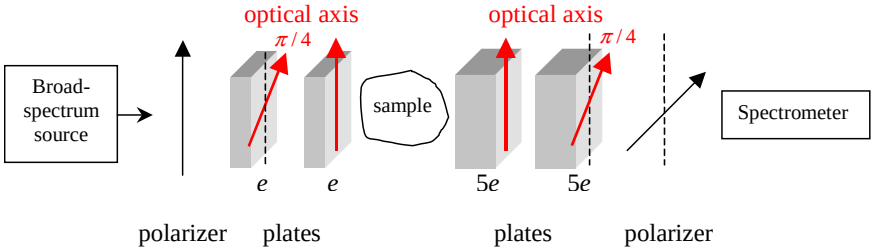

Fig. 1. Snapshot Mueller polarimeter for the configuration (*e*, *e*, 5*e*, 5*e*).

The thickness of each birefringent plate is a crucial parameter to go back to the Mueller matrix. In fact, many configurations can be used [9] and we have chosen to build a snapshot polarimeter with the scheme (*e*, *e*, 5*e*, 5*e*), i.e. an encoding system made of two identical birefringent plates whose thickness is *e*, and a decoding system made of two identical birefringent plates whose thickness is 5*e*. The choice of the thickness is discussed at the end of this section.

Let $[P(\theta)]$and $[B(\phi,\theta)]$ be respectively the Mueller matrix at angle θ for a polarizer and a birefringent plate whose retardation is ϕ. By using the Stokes-Mueller formalism, the action of the snapshot polarimeter can be written on an input Stokes vector $\vec{S}_i$

$$\vec{S}_o = \left[P(\pi/2)\right].\left[B(5\phi,\pi/4)\right].\left[B(5\phi,0)\right].[M].\left[B(\phi,0)\right].\left[B(\phi,\pi/4)\right].\left[P(0)\right].\vec{S}_i, \qquad (1)$$

$$\phi = \frac{2\pi\,\Delta n_{(\lambda)}\,e}{\lambda}, \qquad (2)$$

where $[M]$ is the Mueller matrix of the unknown sample, Δn is the birefringence of the wave plates, e is the length of the birefringence section of the first plate and λ the wavelength of the light. In our case, as the analysis of the signal is made on a narrow spectrum range ($\Delta\lambda \approx 10\,\text{nm}$), the retardation can be expressed in the first-order approximation

$$\phi \approx \phi_0 + f_0\,\lambda, \qquad (3)$$

and the intensity measured by the spectrometer is equal to

$$\begin{aligned}32\,I(\lambda) = {} & 8m_{00} + 4m_{02} - 4m_{20} - 2m_{22} + (8m_{01} - 4m_{21})\cos(f_0\lambda) \\ & -(4m_{02} - 2m_{22})\cos(2f_0\lambda) + 2m_{12}\cos(3f_0\lambda) - 4m_{11}\cos(4f_0\lambda) \\ & -(8m_{10} + 4m_{12})\cos(5f_0\lambda) - 4m_{11}\cos(6f_0\lambda) + 2m_{12}\cos(7f_0\lambda) \\ & -(m_{22} - m_{33})\cos(8f_0\lambda) + 2m_{21}\cos(9f_0\lambda) + (4m_{20} + 2m_{22})\cos(10f_0\lambda) \\ & + 2m_{21}\cos(11f_0\lambda) - (m_{22} + m_{33})\cos(12f_0\lambda) - (4m_{03} - 2m_{23})\sin(2f_0\lambda) \\ & - 2m_{13}\sin(3f_0\lambda) + 2m_{13}\sin(7f_0\lambda) + (m_{23} + m_{32})\sin(8f_0\lambda) - 2m_{13}\sin(9f_0\lambda) \\ & -(4m_{30} + 2m_{32})\sin(10f_0\lambda) - 2m_{31}\sin(11f_0\lambda) - (m_{23} - m_{32})\sin(12f_0\lambda), \end{aligned} \quad (4)$$

where m_{ij} (i, j=0,..,3) are the coefficients of the Mueller matrix for an unknown sample.

The choice of the thickness in our set-up leads to the generation of 12 frequencies which are integer multiples of the fundamental frequency f_0. The Fourier transform of the signal $I(\lambda)$ then creates 12 peaks in real and imaginary parts whose magnitudes are expressed as a linear combination of m_{ij} coefficients (Table.1).

Table 1. Magnitude of Real and Imaginary Peaks According to m_{ij} Coefficients.

Real Part		Imaginary Part	
Frequency	Magnitude (x 64)	Frequency	Magnitude (x 64)
0	$16m_{00} + 8m_{02} - 8m_{20} - 4m_{22}$	0	0
f_0	$8m_{01} - 4m_{21}$	f_0	0
$2f_0$	$-4m_{02} + 2m_{22}$	$2f_0$	$-4m_{03} + 2m_{23}$
$3f_0$	$2m_{12}$	$3f_0$	$-2m_{13}$
$4f_0$	$-4m_{11}$	$4f_0$	0
$5f_0$	$-8m_{10} - 4m_{12}$	$5f_0$	0
$6f_0$	$-4m_{11}$	$6f_0$	0
$7f_0$	$2m_{12}$	$7f_0$	$2m_{13}$
$8f_0$	$-m_{22} + m_{33}$	$8f_0$	$m_{23} + m_{32}$
$9f_0$	$2m_{21}$	$9f_0$	$-2m_{31}$
$10f_0$	$4m_{20} + 2m_{22}$	$10f_0$	$-4m_{30} - 2m_{32}$
$11f_0$	$2m_{21}$	$11f_0$	$-2m_{31}$
$12f_0$	$-m_{22} - m_{33}$	$12f_0$	$-m_{23} + m_{32}$

To retrieve the m_{ij} coefficients, a 25-dimension vector $\vec{V}$, whose components are the magnitude of the peaks, is defined as

$$\vec{V} = \left[V_0^{\mathrm{Re}} \quad V_1^{\mathrm{Re}} \quad V_2^{\mathrm{Re}} \quad \ldots \quad V_{12}^{\mathrm{Re}} \quad V_1^{\mathrm{Im}} \quad V_2^{\mathrm{Im}} \quad \ldots \quad V_{12}^{\mathrm{Im}} \right]^T, \quad (5)$$

where $[\ ]^T$ represents the transpose of a matrix, and the m_{ij} are put in a 16-dimension vector $\vec{X}$ as follows

$$\vec{X} = [m_{00} \quad m_{01} \quad m_{02} \quad m_{03} \quad ... \quad m_{30} \quad m_{31} \quad m_{32} \quad m_{33}]^T . \tag{6}$$

From Table 1, the 25×16 dimension transformation matrix $[P]$ can be found for which we have

$$\vec{V} = [P].\vec{X}, \tag{7}$$

and the measurement of $\vec{V}$ provides the m_{ij} coefficients by the relationship

$$\vec{X} = ([P]^T.[P])^{-1}.[P]^T.\vec{V}. \tag{8}$$

Many configurations allow this inversion of the system. The configuration (e, e, 5e, 5e) has the advantage of providing equidistant peaks in the Fourier domain. Nevertheless an other theoretical configuration (2e, e, 7e, 14e) provides the greatest number of equations (equidistant peaks generated from f_0 to $24\,f_0$) but, in practice, it would generate too high frequencies which could make it difficult to measure peak magnitudes because of the response of the detection.

At last, we must also note that the model assumes the m_{ij} coefficients to be independent of the wavelength.

3. Experimental set-up and corrections

The source is a super luminescent diode with a 15 nm-broadband spectrum around the wavelength $\lambda_0 = 829\,\text{nm}$. The signal of the snapshot polarimeter is measured with a grating of 1200 lines/mm and a 512×512 pixel CCD camera whose spectrum coverage is about 10 nm. For this range, we can reasonably assume that the m_{ij} coefficients are independent of the wavelength.

The choice of the material and the thickness for the birefringent plates must respect two conditions. On the one hand, the fundamental frequency f_0 has to be high enough to perform a Fourier transform with a satisfactory accuracy. On the other hand, the highest frequency $12\,f_0$ has to be small enough for the magnitude of the related peak not to be dwindled by the response of the detection. So, we decided to use calcite plates ($\Delta n(\lambda_0)$=0.166) with a thickness $e = 2.08 \pm 0.01\,\text{mm}$ for the coding plates and $5e = 10.4 \pm 0.01\,\text{mm}$ for the decoding plates. The major interest of the calcite is its high birefringence that permits the use of reasonably thick plates. With this configuration we get 7 sampled points per period for the $12f_0$-frequency, which largely respects Nyquist criteria.

Fig. 2 shows the measured spectrum $I(\lambda)$ for a vacuum measurement, i.e. without any sample, and compares it to the theoretical spectrum based on the model. We have suppressed the shape of the spectrum for the experimental signal by using the Flat Field function on the spectrometer.

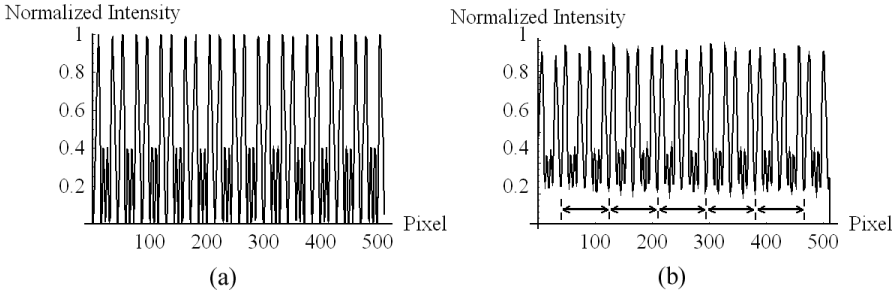

Fig. 2. Theoretical (a) and experimental (b) signals given by the snapshot Mueller polarimeter. The experimental signal is split into 5 zones for which the instantaneous frequency will be studied.

Differences between the two signals require us to make several corrections.

For a start, we notice that the experimental signal has a lower contrast than the theoretical signal. This is due to the response of the detection which reduces the amplitude of high frequencies because of pixel size and the spectrometer slit. The response of the detection has been measured by comparing the height of peaks in the Fourier domain for both theoretical and experimental signals obtained from vacuum (Fig. 3). The $12f_0$-frequency peak is reduced by more than half for our device, which shows that the choice of the wave plate thickness is not restricted by the sampling but by pixel size

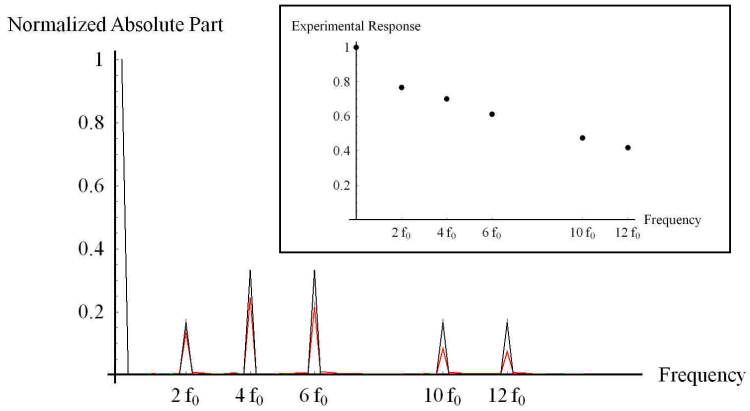

Fig. 3. Theoretical (black) and experimental (red) absolute values of the Fourier transform for vacuum. The inset graph shows the experimental response of the detection from the vacuum signal.

Moreover, we can observe from Fig. 2 that the intensity according to CCD pixels is not exactly a periodic signal. Indeed the period is slightly different for each zone (Fig. 4) due to the nonlinear relationship between retardation ϕ and wavelength from (2) and, to a smaller degree, because of the index law of the birefringent plates in the spectral window analysis [10], the birefringence going down from 0.16618 to 0.16601 on the analysis window (10 nm).

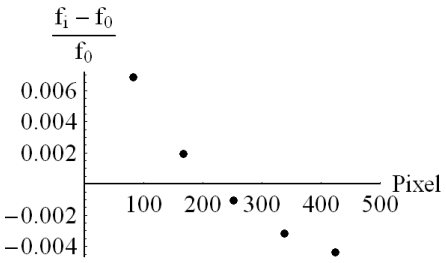

Fig. 4. Relative evolution of the instantaneous frequency f_i in each zone defined in Fig. 2. b.

On the other hand, the experimental signal differs from the theoretical one because the thickness of the four wave plates does not correspond exactly to the theoretical scheme (e, e, 5e, 5e). Indeed, owing to the accuracy of the calcite cut, the wave plates are rotated to adjust the optical path but there are still errors that must be measured. The theoretical scheme then becomes (e, e+e_2, 5e+e_3, 5e+e_4) for which e_2, e_3, and e_4 are respectively the thickness errors of the second, third, and fourth wave plate, the first wave plate setting the reference thickness. These errors can be written in the form of phase errors ϕ_2, ϕ_3, and ϕ_4 respectively and the output Stokes vector is expressed as

$$\vec{S}_o = \left[P(\pi/2)\right].\left[B(5\phi+\phi_4,\pi/4)\right].\left[B(5\phi+\phi_3,0)\right].[M] \\ .\left[B(\phi+\phi_2,0)\right].\left[B(\phi,\pi/4)\right].\left[P(0)\right].\vec{S}_i. \quad (9)$$

For vacuum, the intensity results in

$$16I(\lambda) = 3+\cos\left[2(\phi_w + f_0\lambda)+\phi_2+\phi_3-\phi_4\right]-2\cos\left[4(\phi_w + f_0\lambda)+\phi_4\right] \\ -2\cos\left[6(\phi_w + f_0\lambda)+\phi_4\right]+\cos\left[10(\phi_w + f_0\lambda)+\phi_2+\phi_3+\phi_4\right] \\ -\cos\left[12(\phi_w + f_0\lambda)+\phi_2+\phi_3+\phi_4\right], \quad (10)$$

where ϕ_w comes from the position of the analysis window in which ϕ_0 has been included to simplify the formula. Thus if phase errors ϕ_2, ϕ_3, and ϕ_4 exist, whatever the position of the analysis window, the Fourier transform of the signal leads to peaks whose imaginary part is not null, as shown in Fig. 5.

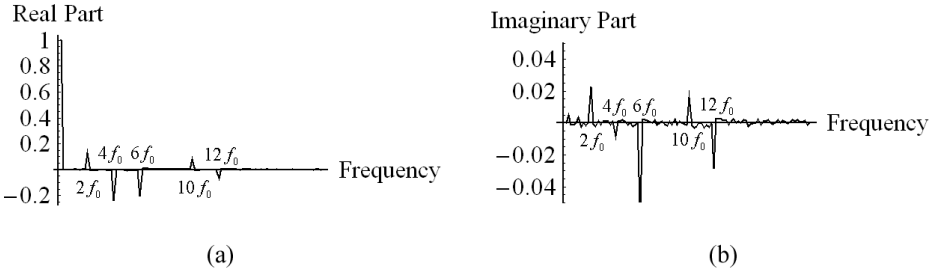

(a) (b)

Fig. 5. Fourier transform of the experimental signal of vacuum. (a) Real Part. (b) Imaginary Part.

From the measurement of the argument for each peak (Fig. 5) and Eq. (10), it is then possible to go back to phase errors. Nevertheless the signal for vacuum is not sufficient to measure errors, as only ϕ_2+ϕ_3 and ϕ_4 can be found. So, using a linear polarizer instead, with π/4

orientation for instance, enables to determine completely the phase errors and to calculate the corrected transformation matrix [*P*] associated to Eq. (9).

Finally, to improve the retrieval of m_{ij} coefficients, we can analyze the imaginary part of peaks versus the position of the analysis window (Fig. 6).

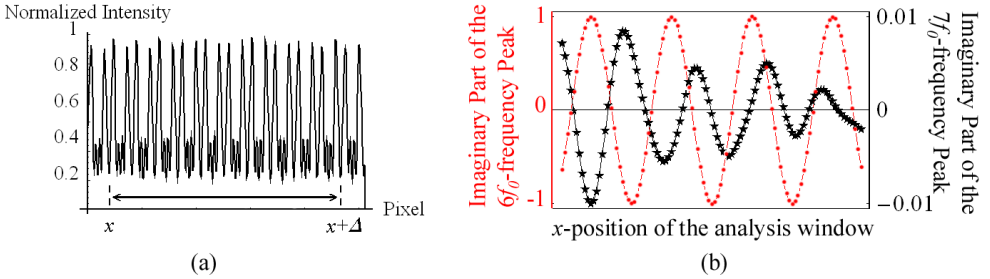

Fig. 6. (a) The analysis window, whose length is Δ, is positioned at the pixel x for vaccum. (b) According to the analysis window position, the imaginary parts of the $6f_0$-frequency peak (red points) and of the $7f_0$-frequency peak (black asterisks) are measured. For vacuum, we expect the snapshot Mueller polarimeter to get a $6f_0$-frequency peak and no $7f_0$-frequency peak.

If there is actually a peak, the imaginary part versus the analysis window corresponds to a sinusoidal function whose frequency is equal to the frequency of the peak. If not, the imaginary part is not well fitted by a sinusoidal function, which permits us to assume that the absolute value of the peak is equal to zero. This noise filter is less effective if the signal is very noisy, which can lead to mistakes for small values of m_{ij}, so it must be used with caution.

4. Experimental Mueller matrices

In this section we present the experimental Mueller matrices for two standard media: vacuum (Table 2) and a linear polarizer aligned by a step-by-step motor with an accuracy of 0.01° (Table 3). These results are the first measurements obtained by a snapshot Mueller polarimeter. Both have been obtained from a single acquisition of 1 ms and we have found that experimental Mueller matrices differ from the theoretical matrices. In order to eliminate the systematic errors, some corrections must be carried out such as the response of the detector and the adjustment of the plates described in section 3. Nevertheless some significant errors still remain - 2% for vacuum and 8% for a linear polarizer at $\pi/6$. In order to know if these differences came from systematic errors and random errors, a statistical treatment has been carried out with 100 data acquisitions. For an acquisition time of 1ms the maximum standard deviation on coefficients is then equal to 0.005, which shows that the residual errors are systematic errors which are not totally compensated by correction methods.

Thus, the m_{ij} retrieval is very dependent on the systematic errors and their importance increases with the complexity of the signal. Indeed, the polarizer at 0° only has 5 peaks in the Fourier domain whereas the polarizer at $\pi/6$ has 12 peaks, i.e. the maximum number of peaks. A part of the systematic errors could be due to the weak sampling (only 512 pixels) which might affect the measurement of phase errors ϕ_2, ϕ_3 and ϕ_4, and the response of the spectrometer.

Table 2. Experimental Mueller Matrix for Vacuum Obtained from a Single Acquisition of 1 ms with and without Corrections.

Corrections	Experimental Mueller Matrix
without any corrections	$\begin{pmatrix} 1 & 0.026 & -0.245 & 0.002 \\ 0.028 & 0.899 & 0.012 & -0.006 \\ 0.053 & 0.007 & 0.565 & 0.171 \\ 0.053 & 0.006 & -0.18 & 0.554 \end{pmatrix}$
+ response of the detection	$\begin{pmatrix} 1 & 0.024 & -0.005 & 0.069 \\ 0.029 & 0.992 & 0.017 & -0.006 \\ 0.022 & 0.011 & 0.956 & 0.292 \\ 0.097 & 0.009 & -0.304 & 0.941 \end{pmatrix}$
+ phase error correction	$\begin{pmatrix} 1 & 0.024 & 0.004 & -0.02 \\ 0.03 & 1.009 & 0.01 & -0.017 \\ 0.007 & 0.013 & 1.002 & -0.002 \\ 0.012 & 0.005 & -0.017 & 1.001 \end{pmatrix}$
+ noise filter	$\begin{pmatrix} 1 & 0 & 0.002 & -0.016 \\ 0 & 1.007 & 0 & 0 \\ 0.009 & 0 & 0.999 & 0.007 \\ 0.008 & 0 & -0.007 & 0.999 \end{pmatrix}$

Table 3. Experimental Mueller Matrix (1ms) for Different Positions of a Linear Polarizer after Corrections: Response of the Detector + Phase Error Correction + Noise Filter.

	Theory	Experiment
Polarizer (0°)	$\begin{pmatrix} 1 & 1 & 0 & 0 \\ 1 & 1 & 0 & 0 \\ 0 & 0 & 0 & 0 \\ 0 & 0 & 0 & 0 \end{pmatrix}$	$\begin{pmatrix} 1 & 0.993 & 0 & 0 \\ 1.018 & 1.001 & 0 & 0 \\ 0 & 0 & 0 & 0 \\ 0 & 0 & 0 & 0 \end{pmatrix}$
Polarizer (π/2)	$\begin{pmatrix} 1 & -1 & 0 & 0 \\ -1 & 1 & 0 & 0 \\ 0 & 0 & 0 & 0 \\ 0 & 0 & 0 & 0 \end{pmatrix}$	$\begin{pmatrix} 1 & -1.014 & 0 & 0 \\ -0.989 & 0.996 & 0 & 0 \\ 0 & 0 & 0 & 0 \\ 0 & 0 & 0 & 0 \end{pmatrix}$
Polarizer (π/6)	$\begin{pmatrix} 1 & 0.500 & 0.866 & 0 \\ 0.500 & 0.250 & 0.433 & 0 \\ 0.866 & 0.433 & 0.75 & 0 \\ 0 & 0 & 0 & 0 \end{pmatrix}$	$\begin{pmatrix} 1 & 0.489 & 0.829 & 0.027 \\ 0.508 & 0.255 & 0.390 & -0.037 \\ 0.860 & 0.416 & 0.726 & -0.017 \\ -0.013 & 0.008 & 0.073 & 0.012 \end{pmatrix}$

5. Conclusion

The validity of the snapshot Mueller polarimeter is proved experimentally. We have measured full Mueller matrices of two different media in 1 ms with a maximum absolute error of nearly 0.08 on coefficients. The retrieval of the m_{ij} is very dependent on systematic errors. The accuracy and the time of our measurements could be widely improved by using a better-adapted spectrometer (sampling and acquisition time).

Acknowledgments

The authors thank Mr. G. Zion for technical assistance in achieving the mechanical items and Mr. M. Koabaz for his help in the set-up.